Pergamon

Materials Research Bulletin 35 (2000) 2287–2294

Materials Research Bulletin

Synthesis and characterization of Li–Mn–V–O spinel as cathode material for lithium battery applications

K.R. Murali*, T. Saravanan, S. Anand Venkatesh, V. Ganesh

Electrochemical Materials Science Division, Central Electrochemical Research Institute, Karaikudi 630 006, India

(Refereed)
Received 10 February 2000; accepted 11 April 2000

Abstract

A low temperature sol-gel technique was employed for the synthesis of vanadium substituted spinel of the type $LiMn_{2-x}V_xO_4$ (x = 0.1 to 0.5). X-ray diffraction data indicates evidence for substitution of vanadium in the lattice. Particle size, FTIR, and differential thermal analyses were carried out on the samples. Charge–discharge characteristics of cells fabricated using these materials were studied. The cells were found to be stable for more than 20 cycles.

Keywords: A. Oxides; B. Sol-gel chemistry; C. X-ray diffraction; D. Energy storage

1. Introduction

In recent years, first-row alkali transition metal oxides have been extensively used as cathode materials for lithium rechargeable battery applications. Among these, $LiCoO_2$ [1], $LiNiO_2$ [2], and spinel $LiMn_2O_4$ [3–5] are the best choices for commercialization of lithium batteries because of their high voltage, high capacity, high energy density, and cycleablity. $LiMn_2O_4$-based spinel oxides are better candidates than the other existing cathode materials. However, on cycling, the octahedral high-spin Mn^{3+} cation tends to be localized and, hence, causes destabilization of crystal geometry, resulting in fading of capacity. To overcome this Jahn–Teller distortion, substitution of mixed valence metals such as Ni, Co, Zn, Cu, and V have been attempted. While reports are available on Ni, Co, and Cu substituted systems

* Corresponding author.

0025-5408/00/$ – see front matter
PII: S0025-5408(00)00446-3

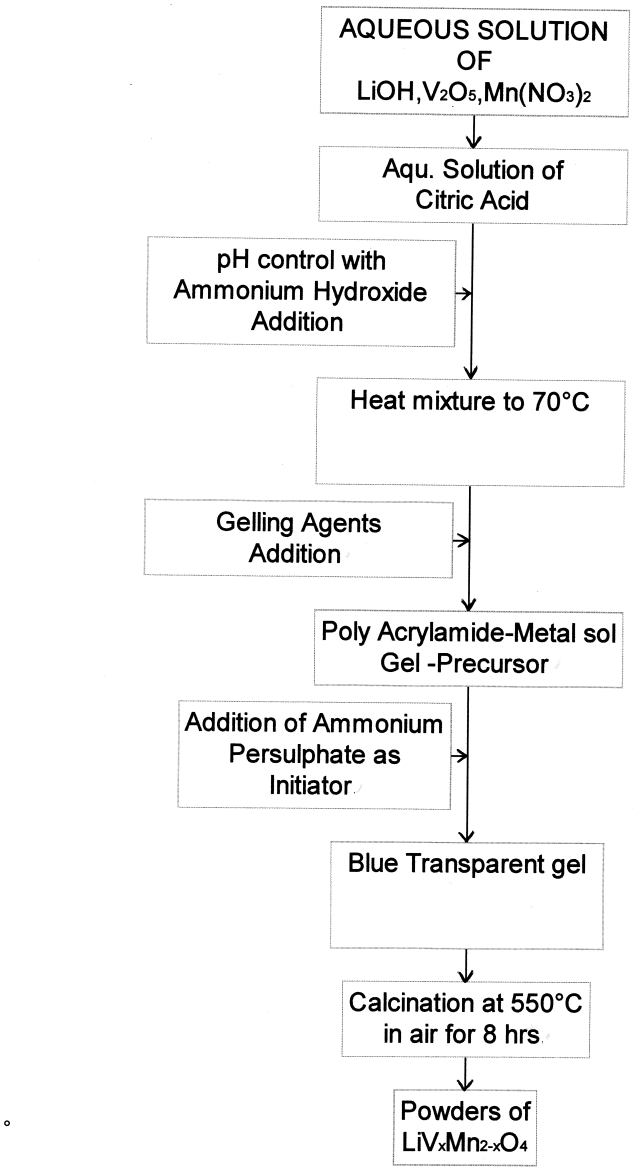

Fig. 1. Flow diagram.

[6–17], to our knowledge, there is no report on single-phase vanadium substituted systems. An earlier study using solid-state preparation technique [18] reported the incorporation of V_2O_5 into $LiMn_2O_4$ spinel matrices. This result may have been due to NH_4VO_3 being used as a precursor, which decomposes to V_2O_5 at about 500°C in the presence of an oxidizing atmosphere. This V_2O_5 thermally decomposes to V_2O_3 in the presence of a reducing atmosphere at 900°C [19]. Hence, the creation of vanadium ion substituted $LiMn_2O_4$ single-phase spinel system was not possible with this preparation technique.

In the present investigation, a new sol-gel route was adopted in which V_2O_5 was

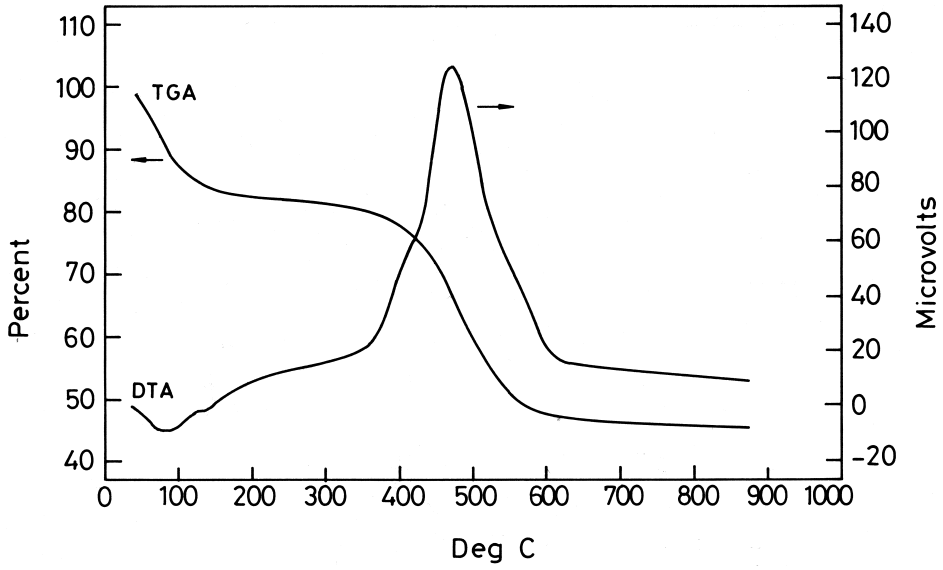

Fig. 2. TGA and DTA scans of the Li–Mn–V–O spinel oxide.

completely dissolved in LiOH, forming vanadates of lithium. This lithium vanadate was reduced with manganese nitrate to form the vanadium substituted $LiMn_2O_4$ spinel oxides [19].

2. Experimental

$LiV_xMn_{2-x}O_4$ powders were prepared according to the procedure shown in the flow diagram (Fig. 1). Stoichiometric amount of LiOH, V_2O_5, and $Mn(NO_3)_2{\cdot}4H_2O$ salts were dissolved in distilled water. An aqueous solution of citric acid was mixed with the metal-ion precursor as a chelating agent. The mixture was stirred continuously and the pH was adjusted in the range of 6–7 by the slow addition of NH_4OH. Gelling agents in the form of monomer-acrylamide and N-N′-methylene-bis-acrylamide, followed by ammonium persulphate, were added to the solution. A transparent blue gel was obtained. The gel was then heated initially at 300°C for about 6 h, to remove the organic material. The resulting powder was calcined at 550°C for 8 h to get a porous black powder. Vanadium-doped cathode material was mixed with conducting carbon black (10 wt%) and PTFE binder (5 wt%) and pressed on a nickel mesh of electrode area 1 cm^2 at a pressure of 5 tons. A SnO_2 electrode served as anode with 1 M $LiClO_4$ in propylene carbonate as the electrolyte. The discharge behavior of vanadium doped ($x = 0.5$) $LiMn_2O_4$ spinel oxide material was studied.

Thermogravimetric/differential thermal analysis (TG/DTA) was carried out, using PL Thermal Science STA 1500, to determine the kinetics of the process and phase formation. The powders were characterized by X-ray diffraction using a JEOL JDX 8030 X-ray diffractometer with Cu Kα radiation. FTIR analysis was done using a Perkin-Elmer 3500 instrument.

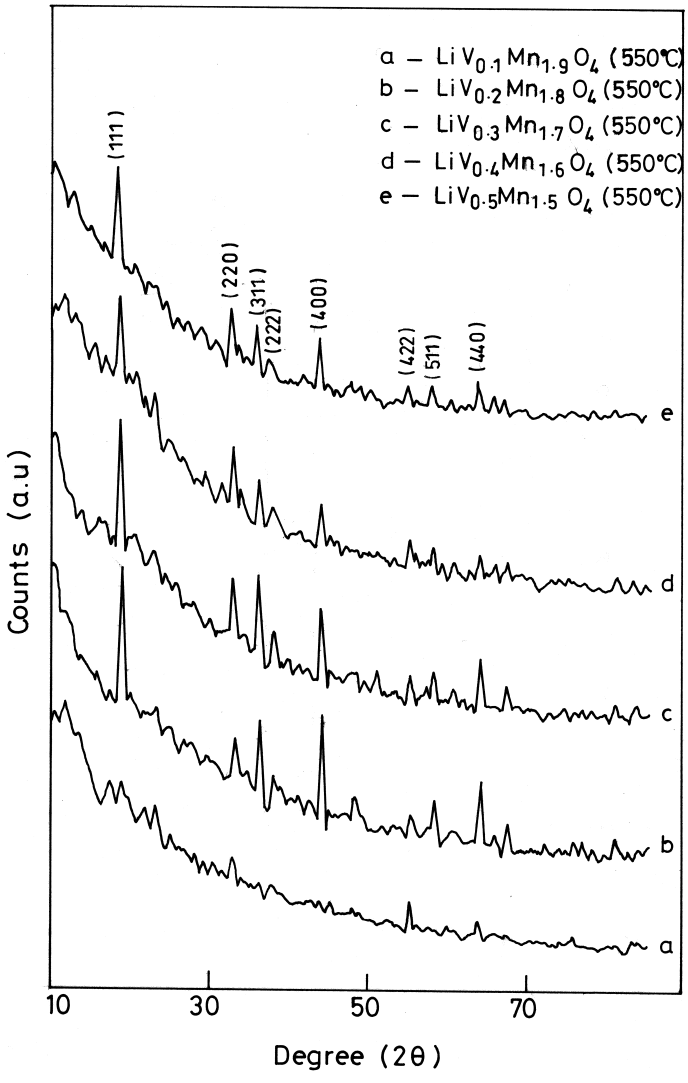

Fig. 3. XRD pattern of $LiV_xMn_{2-x}O_4$ (x = 0.1 to 0.5).

3. Results and discussion

The decomposition kinetics of the preheated samples was deduced from the TGA. From the thermogram (Fig. 2) it is observed that around 81°C water of crystallization is removed with a mass loss of about 20%; a small endothermic peak is also found. At about 469°C, a strong well-defined exothermic peak is observed with a mass loss of about 30%. The TGA curve shows that no mass loss is observed after 550°C, indicating that the crystallization starts and the single phase product is formed.

The XRD patterns (Fig. 3) indicated all the reflections corresponding to $LiV_xMn_{2-x}O_4$ (x = 0.1 to 0.5). Peaks are observed that could be assigned to the (4 0 0) reflection of the

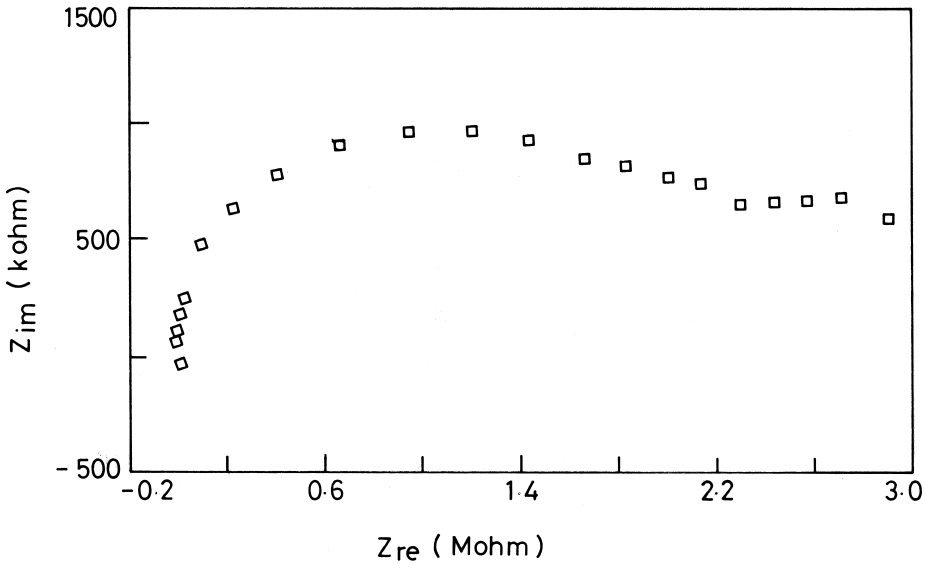

Fig. 4. FTIR spectra of $LiV_xMn_{2-x}O_4$ (x = 0.1 to 0.5).

$LiMn_2O_4$ spinel phase. Further, (2 2 0) and (4 2 2) reflection peaks of the spinel correspond to the vanadium metal-ion at the 8a tetrahedral site and Mn at the 16d octahedral site of a cubic close-packed oxygen framework, respectively [20]. The (2 2 0) reflection peak is characteristic of transition metal-ion substitution into the spinel lattice as reported in the literature [13].

As the concentration of the vanadium incorporation in the Mn site increases from x = 0.1 to 0.5, in the $LiV_xMn_{2-x}O_4$ spinel lattice, the XRD patterns indicate a peak shift to higher angle side. The lattice parameter *a* for different x values was determined. The *a* value slightly decreases from 8.26 Å for x = 0.1 to 8.244 Å for x = 0.5. This behavior represents the topotactic reaction mechanism associated with vanadium doping [20].

Fig. 4 shows the FTIR data. A strong absorption peak is observed around 900 cm^{-1}, which may be due to stretching of (VO_4). Due to symmetric stretching of the (VO_4) tetrahedron, this strong absorption peak was observed in all the compositions ranging from x = 0.1 to 0.5 in $LiV_xMn_{2-x}O_4$. Another stretching vibration is also observed at about 490 cm^{-1}, which is due to (Li–O). As vanadium substitution increases from 0.1 to 0.5 in the

Table 1
Compositional parameters of vanadium doped lithium manganate spinel oxides

Theoretical formula	Li/Mn	V/Mn	Experimentally obtained
$LiV_{0.1}Mn_{1.9}O_4$	0.502	0.052	$Li_{0.95}V_{0.1}Mn_{1.89}O_4$
$LiV_{0.2}Mn_{1.8}O_4$	0.530	0.104	$Li_{0.96}V_{0.19}Mn_{1.81}O_4$
$LiV_{0.3}Mn_{1.7}O_4$	0.565	0.174	$Li_{0.99}V_{0.3}Mn_{1.72}O_4$
$LiV_{0.4}Mn_{1.6}O_4$	0.618	0.256	$Li_{0.99}V_{0.41}Mn_{1.6}O_4$
$LiV_{0.5}Mn_{1.5}O_4$	0.625	0.303	$Li_{0.97}V_{0.47}Mn_{1.55}O_4$

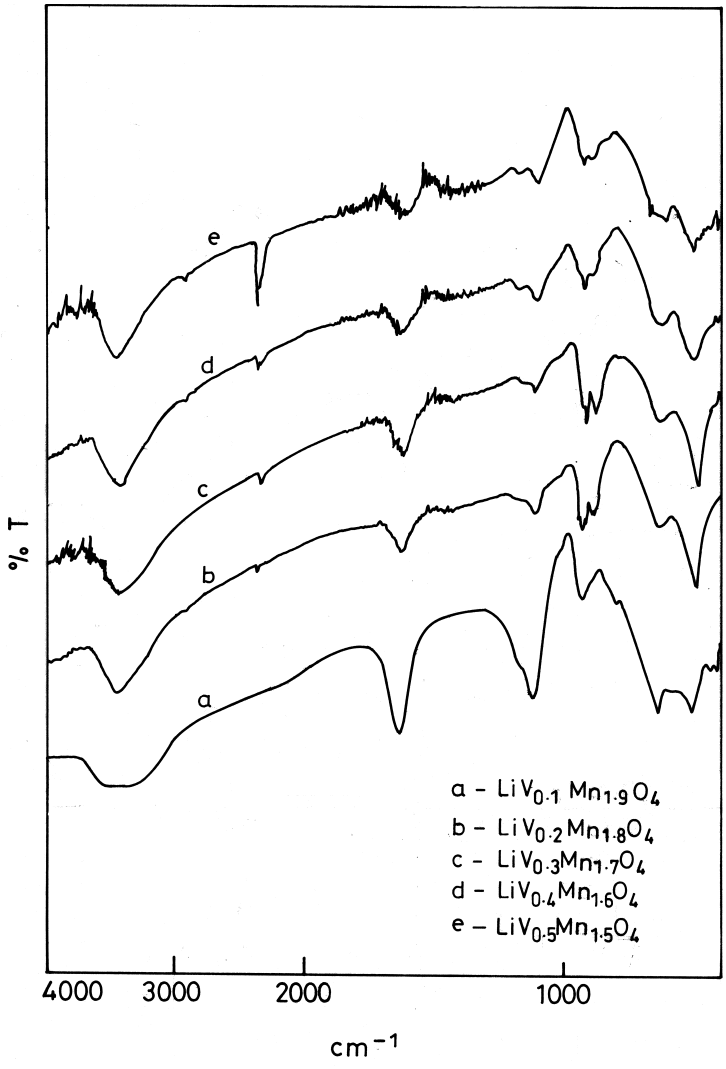

Fig. 5. Impedance behavior of $LiV_{0.3}Mn_{1.7}O_4$ spinel oxide.

Table 2
Variation of charge transfer resistance with vanadium doping

x	$R_{ct}(M\Omega)$
0.1	1.2
0.2	1.6
0.3	2.2
0.4	2.6
0.5	3.2

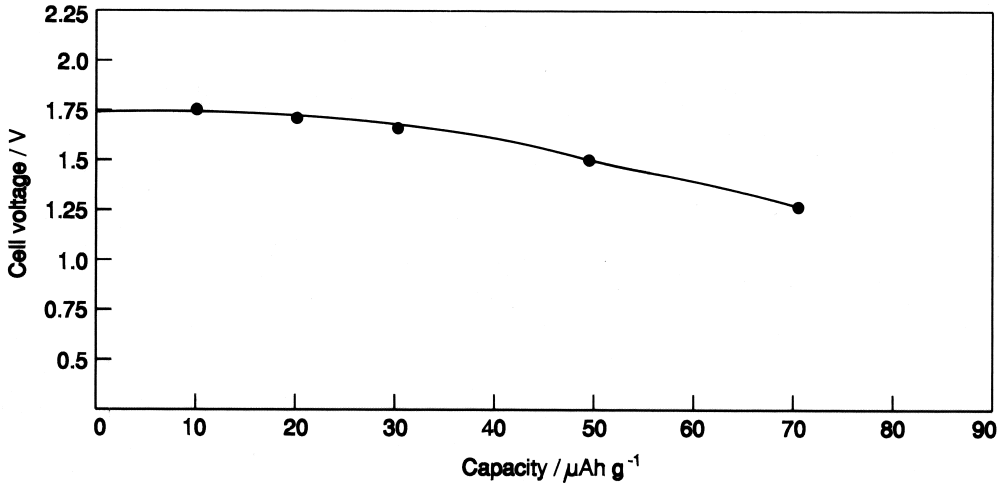

Fig. 6. Voltage profile during first discharge of cell configuration SnO_2/1M $LiClO_4$/$LiV_{0.5}Mn_{1.5}O_4$ at a current density of 10 $\mu A/cm^2$.

parent spinel $LiMn_2O_4$, the absorption bands shifts towards the higher frequency side, indicating the partial substitution of octahedral Mn with the vanadium [21].

The lithium, vanadium, and manganese contents of the samples were determined after dissolving them in a mixture of HCl and HNO_3. The compositions were determined by atomic absorption spectrometry. Chemical analysis results for $LiV_xMn_{2-x}O_4$ (x = 0.1 to 0.5) are summarized in Table 1. The Li/Mn and V/Mn mole ratios obtained from AAS analysis agree well with the mole ratios of the precursors used for the synthesis of $LiV_xMn_{2-x}O_4$ (x = 0.1 to 0.5).

Particle size analysis was performed using a Malvern Instruments EASY particle sizer M3.0. The data shows that about 50% of the particles were between 3 and 10 μm in size, and the remaining particles were between 15 and 28 μm, with a specific surface area of 0.31 m^2/cc.

Impedance analysis was performed using ion-blocking electrodes of EG & G Princeton Applied Research Potentiostat. Pellets 1 cm^2 were prepared under a pressure of 5 tons. The pellets were placed between ion-blocking electrodes such as copper discs and a dc potential of 0 V (OCV) was applied with 5 mV rms ac superimposed. The experiment was carried out in the frequency range 10 Hz to 10 kHz. A typical Nyquist plot for the vanadium substituted (x = 0.3) lithium manganate spinel oxide is given in the Fig. 5. From the plot, the charge-transfer resistance was calculated as R_{ct} = 2.2 MΩ. A fine semi-circle was obtained representing the ideal impedance behavior with frequency. From Table 2 it is evident that as the vanadium content increased from x = 0.1 to 0.5, the charge-transfer resistance increases proportionally, which explains the higher oxidation state of manganese cation with increasing substitution of vanadium.

Fig. 6 shows the voltage profile during the first discharge of cell configuration SnO_2/1M $LiClO_4$/ $LiV_{0.5}Mn_{1.5}O_4$. The OCV of the cell was 1.8 V. In the discharge curve, a plateau was observed around 1.75 V. During the 20th discharge cycle the discharge capacity was

maintained at 70 μAh/g. After the 20th cycle the impedance of the system increases marginally due to the increase in the electrode-electrolyte interfacial resistance. The cell shows a discharge capacity of 70 μAh/g, which gives a coloumbic efficiency of 70%. Further work to increase the coloumbic efficiency of the cathode material is underway.

4. Conclusions

In the present investigation, we demonstrated a new low temperature sol-gel route for the synthesis of vanadium substituted lithium manganate spinel oxides. The synthesis temperature is lower than that of solid-state reaction route reported earlier. Cells fabricated with this material were found to be stable for more than 20 cycles. Further studies on charge–discharge cycling are underway.

References

[1] T. Ohuzuka, M. Kitagawa, T. Hirai, J Electrochem Soc 137 (1990) 760.
[2] D. Guyomard, J.M. Tarascon, Solid State Ionics 69 (1994) 222.
[3] G. Pistoia, G. Wang, C. Wang, Solid State Ionics 58 (1992) 285.
[4] T. Nagaura, M. Yokokawa, T. Hashimoto, U.K. Patent Appl. 2,196,875, 1988.
[5] T. Nagaura, M. Yokokawa, T. Hashimoto, U.S. Patent 4,828,834, 1989.
[6] K. Amine, H. Tukamoto, H. Yasuda, Y. Fujita, J Electrochem Soc 143 (1996) 1607.
[7] Z.L. Liu, A.S. Yu, J.Y. Lee, J Power Sources 74 (1998) 228.
[8] Y. Ein-Eli, W.F. Howard Jr., S.H. Lu, S. Mukerjee, J. McBreen, J.T. Vaughey, M.M. Thackeray, J Electrochem Soc 145 (1998) 1238.
[9] T. Ohzuku, S. Takeda, M. Iwanga, J Power Sources 81–82 (1999) 90.
[10] I.J. Davidson, R.S. McMillan, H. Slegr, B. Luan, I. Kargina, J.J. Murray, I.P. Swainson, J Power Sources 81–82 (1999) 406.
[11] Y.-K. Sun, D.-W. Kim, Y.-M. Choi, J Power Sources 79 (1999) 231.
[12] P. Arora, B.N. Popov, R.E. White, J Electrochem Soc 145 (1998) 807.
[13] H. Kawai, M. Nagata, H. Tukamoto, A.R. West, J Mater Chem 8 (1998) 837.
[14] A. deKoch, E. Ferg, R.J. Gummow, J Power Sources 70 (1998) 247.
[15] F. Lecras, M. Anne, D. Bloch, P. Strobel, Solid State Ionics 106 (1998) 1.
[16] A. Manthiram, J. Kim, Chem Mater 10 (1998) 2895.
[17] Y.-K. Sun, S.-H. Jin, J Mater Chem 8 (1998) 2399.
[18] N. Kumagai, T. Fujiwara, K. Tanno, J Power Sources 43–44 (1993) 635.
[19] Ullmann's Encyclopedia of Industrial Chemistry, VCH, Deerfield Beach, FL, 1996, Vol. 27, p. 380.
[20] Q. Feng, H. Kanoh, Y. Miyai, K. Ooi, Chem Mater 7 (1995) 379.
[21] S.R.S. Prabaharan, M.S. Michael, R.S. Radhakrishna, C. Julien, J Mater Chem 7 (1997) 1791.